의학박사 학위논문

관상동맥 경화반에 작용하는 혈역학적 외력과 병변의 형태적 특징에 따른 혈역학적 외력의 분포에 대한 분석

Analysis of Hemodynamic Force Acting on Coronary Plaque and Its Relationship with Lesion Geometry

2016년 6월

서울대학교 대학원

의학과 내과학 전공

이주명

PhD. Thesis

Analysis of Hemodynamic Force Acting on Coronary Plaque and Its Relationship with Lesion Geometry Using Computational Fluid Dynamics

Brief Title: Analysis of Hemodynamic Forces Acting on Coronary Plaque

Joo Myung Lee, MD, MPH

Guiding Professor: Dae-Won Sohn, MD, PhD

Analysis of Hemodynamic Force Acting on Coronary Plaque and Its Relationship with Lesion Geometry Using Computational Fluid Dynamics

Joo Myung Lee

Department of Medicine

The Graduate School of Medicine

Seoul National University

Abstract

Background: Coronary plaque rupture occurs when plaque stress exceeds plaque strength. We performed this study to characterize the hemodynamic force acting on plaque and to investigate its relationship with lesion geometry.

Methods: Computational fluid dynamics was applied to 114 lesions (81 patients) from coronary computed tomographic (CT) angiography. The axial plaque stress (APS) was computed by extracting the axial component of hemodynamic stress acting on stenotic lesions and the axial lesion asymmetry was assessed by the luminal radius change over length (radius gradient, RG). Lesions were divided into upstream-dominant (upstream RG > downstream RG) and downstream-dominant lesions (upstream RG < downstream RG) according to the RG.

Results: 33 lesions (28.9%) showed net retrograde axial plaque force. Upstream APS linearly increased as lesion severity increased whereas downstream APS exhibited a concave function for lesion severity. There was a negative correlation (r=-0.274, p=0.003) between APS and lesion length. The pressure gradient, CT-derived fractional flow reserve (FFR_{CT}), and wall shear stress (WSS) were consistently higher in upstream segments, regardless of the lesion asymmetry. However, APS was higher in the upstream segment of upstream-dominant lesions (11371.96 ± 5575.14 vs. 6878.14 ± 4319.51 dyne/cm^2, p<0.001), and in the downstream segment of downstream-dominant lesions (7681.12 ± 4556.99 vs. 11990.55 ± 5556.64 dyne/cm^2, p<0.001). Although there were no differences in FFR_{CT}, % diameter stenosis and WSS pattern, the distribution of APS was different between upstream- and downstream-dominant lesions.

Conclusion: APS uniquely characterizes the stenotic segment and has a strong relationship with lesion geometry. Clinical application of these hemodynamic and geometric indices may be helpful to assess the future risk of plaque rupture and to determine treatment strategy for patients with coronary artery disease.

Key Words: coronary artery disease; axial plaque stress; wall shear stress; pressure; coronary plaque; computational fluid dynamics; coronary computed tomography angiography.

Student Number: 2014-30606

Condensed Abstract

The axial plaque stress (APS) distinctively characterizes the distribution of plaque stress according to the lesion geometry even for lesions with the same degree of stenosis severity, pressure change, and fractional flow reserve (FFR). The geometric parameter, radius gradient (RG), incorporates most clinically relevant geometric parameters: lesion length, minimum lumen area, and stenosis severity. The strong correlation between APS and RG can potentially provide an explanation for how plaque rupture occurs downstream segment as well as the upstream segment, and why plaques are more likely to rupture in short focal lesions than in diffuse ones. Therefore, patient-specific evaluation of APS and RG can provide valuable information in identifying lesions exposed to high hemodynamic forces, and determining improved treatment strategies for patients with coronary artery disease.

Table of Contents

1.	Abstract	3
2.	Condensed Abstract	5
3.	Abbreviations	7
4.	Introduction	8
5.	Methods	10
6.	Results	17
7.	Discussion	23
8.	Conclusions	29
9.	Abstract (Korean)	30
10.	Acknowledgements	36
11.	References	37
12.	Figure Legend	40
13.	Tables	46
14.	Figures	52

Abbreviations List

APS = axial plaque stress

CFD = computational fluid dynamics

cCTA = coronary computed tomographic angiography

CT = computed tomography

MLA = minimal lumen area

FFR = invasive fractional flow reserve

FFR_{CT} = coronary CT angiography-derived fractional flow reserve

RG = radius gradient

WSS = wall shear stress

Introduction

Coronary plaque rupture is a critical event that triggers the initiation of acute coronary syndrome (ACS). Although the sequence of plaque rupture is well-understood with previously reported histopathological data (1), the prediction of plaque rupture in an individual patient is still problematic. To assess the risk of ACS, image-based findings such as cap thickness, presence of a lipid core and the degree of inflammation have been proposed as the key features of vulnerable plaques (2). However, plaque rupture can occur whenever plaque stress exceeds the plaque strength in a similar mechanism to general mechanical material failures (3,4). Therefore, if the imbalance between plaque durability and external force can be assessed simultaneously, prediction of the risk of plaque rupture can be more accurate.

Among various hemodynamic forces, wall shear stress (WSS) has been proposed as a key hemodynamic force affecting the initiation, progression, and transformation of atherosclerotic plaque from a stable to unstable phenotype (1,3,5,6). However, the magnitude of WSS is significantly smaller than other components of hemodynamic forces such as pressure and thus WSS alone may not act as a direct force for the occurrence of plaque rupture. The coronary arteries are under circumferential and axial tension resulting from blood pressure. A net anterograde axial force on the plaque (largely due to the pressure gradient) would increase the axial tension and plaque stress on the upstream segment of the plaque but decrease those acting on the downstream end of the plaque. The converse is true

for a net retrograde axial force on the plaque, which, paradoxically, can occur for certain plaque geometries despite the minimal pressure gradient acting on the downstream segment of a plaque. These net axial forces may explain the clinical observation that plaque rupture occurs on both upstream and downstream segments of a plaque (7,8).

Recent advances in coronary CT angiography (cCTA) and computational fluid dynamics (CFD) technologies enable quantification of hemodynamic forces acting on plaques with more accurate patient specific geometric models and physiologic boundary conditions than have been possible heretofore (9).

The purpose of this study was to characterize the hemodynamic forces acting on coronary plaques and to investigate its relationship with lesion geometry using CFD applied to coronary models created from cCTA data of patients with coronary artery disease.

Methods

Patient Population

A total of 81 patients presenting with stable angina and suspected coronary artery disease were included for this study from 4 cardiovascular centers in Korea and Japan (Table 1). The inclusion criteria were patients with stable angina, and the existence of cCTA, invasive coronary angiography, and fractional flow reserve (FFR) measurement within an interval of less than 3 months between cCTA and invasive procedures. The study protocol was approved by the institutional review boards of each site, and was in accordance with the Declaration of Helsinki. (ClinicalTrials.gov Identifier: NCT01857687)

Invasive Coronary Angiography and Invasive Fractional Flow Reserve

Selective invasive coronary angiography was performed by standard techniques. All angiograms were reviewed at a core laboratory in a blinded fashion. The FFR was measured using a 0.014-inch pressure-monitoring guidewire (St. Jude Medical, Uppsala, Sweden) in vessels with coronary artery disease. Maximal hyperemia was induced with a continuous intravenous infusion of adenosine or ATP at the rate of 140 μg/kg/min.

Image Acquisition of Coronary CT Angiography

The cCTA images were obtained in accordance with the Society of Cardiovascular Computed Tomography Guidelines on Performance of cCTA, with 64- or higher detector row scanner platforms (10). Oral beta-blockers were administered for any subjects with a heart rate ≥65 beats per minute. Immediately before the cCTA acquisition, 0.2 mg sublingual nitroglycerin was administered.

CFD Analysis of the Lesion in Patients with Coronary Artery Disease

Coronary models constructed from cCTA were discretized into volumetric meshes for CFD analysis. The boundary conditions of CFD domain were assigned on the basis of vessel sizes at each outlet assuming a hyperemic condition as described by Taylor et al (9). Briefly, the basal outlet resistances at rest were determined from the fundamental form-function relationships relating organ flow with organ size according to metabolic demands. Specifically, an allometric scaling law was used to estimate the total coronary flow based on myocardial mass and a morphometry law was used to relate the resistance of the microcirculation downstream of a vessel to the vessel size at each outlet. Then the outlet resistance was reduced by utilizing a mathematical model of hyperemic condition derived from the effect of adenosine on reducing the resistance of the coronary microcirculation. Finally, CFD analysis was performed on the discretized model of geometry with boundary conditions, to numerically solve the governing equations of fluid dynamics as a Newtonian fluid. The numerical solutions of flow and

pressure fields were then used to compute hemodynamic forces on complete spatial domain of geometry including traction and wall shear stress (9).

Stenotic lesions were determined by a visual angiographic evaluation (>30% stenosis) and corresponding lesions were identified in cCTA images. To understand the regional variation of hemodynamic characteristics, each stenotic lesion was subdivided into upstream and downstream segments with respect to the location of minimal lumen area (MLA). Hemodynamic parameters including FFR from cCTA (FFR_{CT}), WSS, pressure, pressure change over length (pressure gradient), traction and axial plaque force were computed from CFD analysis. All cCTA-based geometry constructions and CFD analyses were performed by a single core laboratory, HeartFlow, Inc. (Redwood City, CA, USA).

Analysis of Hemodynamic Forces

The internal stress and strain within the plaque would ultimately affect the plaque rupture, but this internal stress and strain is directly related to the external force, i.e. a high external force increases the internal stress in the plaque. The total force acting on plaques or luminal surfaces is the traction force. If the traction force is divided by the area on which it acts, the term is then called the traction with units of force per unit area. A typical decomposition of traction is with respect to the normal direction of the luminal surface, resulting in the well-known WSS – the tangential component of traction – and pressure – the normal component of traction.

Since the pressure drop mainly occurs in the direction of the vessel across stenotic lesions, i.e. axially, another way to decompose traction is based on the centerline direction of the vessel. This approach of decomposing hemodynamic forces introduces a hemodynamic index: axial plaque stress (APS) (Figure 1). The APS can be computed by the projection of traction onto the centerline of the coronary artery as follows:

$$\overrightarrow{\boldsymbol{APS}} = (\vec{\boldsymbol{t}} \cdot \vec{\boldsymbol{c}})\vec{\boldsymbol{c}}$$

where $\vec{\boldsymbol{t}}$ is the traction vector, $\vec{\boldsymbol{c}}$ is the unit tangential vector of centerline ($\|\vec{\boldsymbol{c}}\| = 1$), and $(\vec{\boldsymbol{t}} \cdot \vec{\boldsymbol{c}})$ is the dot product of $\vec{\boldsymbol{t}}$ and $\vec{\boldsymbol{c}}$. The radial component of traction was not analyzed in this study as the axial component is expected to be the more relevant contributing factor of force imbalance than the radial component since the main driving force caused by pressure gradient is along the vessel length in the axial direction.

APS represents a fluid stress imparted to the surface of the plaque and is the main contributor for the imbalance of force across the lesion. The imbalance of external hemodynamic forces ultimately influences the stress within the plaque and APS uniquely characterizes the stress acting on the upstream and downstream segments of a plaque (Figure 1).

The shape of each upstream and downstream segment in the axial direction would affect the direction and magnitude of the APS. Thus we devised a geometric descriptor to quantitatively describe the axial changes in the legion geometry: radius

gradient (RG). The RG was defined by the radius change over lesion length, where radius change refers to the difference between lesion starting (or ending) point radius and the radius at the location of MLA, and lesion length is defined by the length from the lesion starting (or ending) point to MLA location (Figure 2A). Lesions with steeper radius change in upstream than downstream (i.e., $RG_{upstream} > RG_{downstream}$) were referred to as "upstream-dominant" lesions, whereas those with steeper radius change in downstream than upstream (i.e., $RG_{downstream} > RG_{upstream}$) were referred to as "downstream-dominant" lesions. To account for local variations in lesion shape, RG was also analytically computed by the average of the radius change over infinitesimal intervals, i.e., analytic RG (Figure 2B). In patient lesions, those two definitions of RG were utilized to investigate its relationship with hemodynamic parameters.

Idealized Stenosis Model

In this study, we evaluated the hemodynamic forces acting on coronary plaques and investigated its relationship with lesion geometry using computational fluid dynamics (CFD) technologies in patient-specific lesions. Although recent advances in CFD technologies enabled quantification of hemodynamic forces acting on plaques, nonetheless, diverse clinical presentation, substantial inter-individual heterogeneities in parameters of circulatory system, and presence of many confounding factors in real patients have been major obstacles to elucidating the

complex mechanism of plaque rupture. Therefore, we meticulously devised idealized stenosis models based on realistic ranges of geometric parameters. In order to provide intuitive and simplified explanation of the results from patient lesions, all of the analyses were repeated with idealized stenosis model.

Idealized Stenosis Model Construction

To investigate the variation of hemodynamic forces according to lesion shapes, idealized stenosis models were created by varying the degree of diameter stenosis from 30% to 80% with 10% increment, and varying reference vessel diameters from 2.5 to 4.0 mm with 0.5 mm increment (n= 264). The shape of the lesion was controlled by a sinusoidal function to ensure the smoothness of lesions and MLA was located at 40 mm distal to the inlet of 100 mm long models. The degree of lesion asymmetry was adjusted by changing the upstream and downstream segmental length from 4:1 to 1:4 ratios. Subsequently, radius gradient (RG) of each stenosis model was varied according to the asymmetric shape of lesions. Various hemodynamic forces were derived from coronary flow simulations using the same physiologic boundary conditions as in the patient population herein.

Statistical Analysis

Categorical variables were given as counts and percentages; continuous

variables were described as mean ± standard deviation or median and interquartile range as appropriate. Pearson's correlation coefficients were calculated to determine the relationship among the hemodynamic parameters pertaining to plaque stress and index of plaque geometry. The comparison of segmental hemodynamic forces between upstream and downstream segments in one total plaque was performed with paired-sample t-test. For the comparison of hemodynamic forces between upstream-dominant lesions and downstream-dominant lesions, independent t-sample test was used. The interclass correlation coefficient was used to assess the reliability and agreement between the two different definitions of RG. All statistical analyses were conducted with SPSS version 22.0 (IBM SPSS Statistics, Chicago, IL) and R programming, version 3.0.2 (The R Foundation for Statistical Computing, Vienna, Austria). A two-sided p value <0.05 was considered as significant.

Results

Baseline Characteristics of Patients

A total of 81 patients with 114 non-ostial lesions were enrolled (mean age 63.8 ± 9.0 years, male 85.1%). The median interval between cCTA and invasive coronary angiography were 29 days (interquartile range 13 to 49 days), with no clinical events or revascularization between the tests. The distribution of lesions was: left main to left anterior descending coronary artery (n=72, 64.0%); left circumflex artery (n=19, 16.7%); right coronary artery (n=22, 19.3%). The MLA and % area stenosis by cCTA were 2.01 ± 0.94 mm^2 and 61.98 ± 13.14%, respectively. The mean values of FFR_{CT} and invasive FFR were 0.78 ± 0.12 and 0.79 ± 0.11 (p=0.480), respectively (Table 1).

APS and its Relationship with Stenosis Severity and Lesion Length

The pattern of APS distribution was similar between the data from the patients and from the idealized models (Figure 3). Among the total 114 lesions, 81 lesions (71.1%) showed net anterograde axial plaque force with significantly higher axial plaque force in upstream versus downstream segments (5295.02 ± 3430.43 dyne vs. 3318.04 ± 2298.74 dyne, p<0.001). Conversely, 33 lesions (28.9%) showed net retrograde axial plaque force with significantly higher downstream axial plaque force, compared with upstream segment (2502.25 ± 1365.57 dyne vs. 3766.98 ± 374.38 dyne, p<0.001). In magnitudes, APS ranged up to 30000 dyne/cm^2, while

WSS ranged up to 1000 dyne/cm^2 (Figure 4).

The relationship of APS with pressure gradient is presented in Figure 5. In upstream segments, the APS showed a linear relationship with pressure gradient, but not in downstream segments. Although the pressure gradient in downstream was minimal, the distribution of downstream APS was highly variable. With regard to the relationship with lesion severity, the APS linearly increased as the lesion severity increased in upstream segments. However, downstream APS decreased as stenosis severity exceeded a certain degree. When the stenosis severity was greater than an approximately 60% diameter stenosis, the magnitude of downstream APS was reduced (Figure 6A). The segmental lesion length also affected the APS. A negative correlation (r=-0.274, p=0.003) was observed between the APS and lesion length (Figure 6B).

Relationship of APS with Axial Lesion Asymmetry

In upstream-dominant lesions (n=56, 49.1%), the average RG for upstream and downstream segments were 0.11 ± 0.05 and 0.06 ± 0.03, respectively (p<0.001). In downstream-dominant lesions (n=58, 50.9%), the average RG for upstream and downstream segments were 0.07 ± 0.03 and 0.12 ± 0.05, respectively (p<0.001) (Table 2). In segmental analysis between upstream and downstream segments of stenosis, delta pressure, delta FFR_{CT}, pressure gradient and WSS were consistently higher in upstream segment, regardless of the lesion asymmetry (Table 2). However,

APS exhibited a geometry-dependent distribution. In the upstream-dominant lesions, upstream APS was significantly higher than downstream APS (11371.96 ± 5575.14 vs. 6878.14 ± 4319.51 dyne/cm^2, p<0.001). On the other hand, in the downstream-dominant lesions, the downstream APS was significantly higher than upstream APS (7681.12 ± 4556.99 vs. 11990.55 ± 5556.64 dyne/cm^2, p<0.001) (Table 2). The distribution and differences in hemodynamic parameters according to the plaque geometry showed similar results for a subgroup with more than 40% diameter stenosis (Table 3). When classifying all the lesions into 3 groups, according to the relative balance of RG (upstream-dominant, symmetric, and downstream-dominant), only APS showed concordant differences according to the lesion geometry (Table 4).

Notably, despite no differences in FFR_{CT} (0.83 ± 0.10 vs. 0.80 ± 0.11, p=0.121) or % diameter stenosis (38.58 ± 0.11% vs. 39.48 ± 0.11%, p=0.661) between upstream-dominant and downstream-dominant lesions, the APS distinctively showed significant differences according to lesion geometry. WSS did not exhibit significant difference between the upstream and downstream segments for both groups (upstream WSS: 273.49 ± 181.38 vs. 270.90 ± 124.21, p=0.929; downstream WSS: 147.77 ± 91.84 vs. 153.66 ± 104.89, p=0.750) (Figure 7).

Figure 8 illustrates one representative clinical case with an upstream-dominant lesion and depicts the influence of plaque geometry on APS. The cCTA image was taken when the patient was asymptomatic as part of a routine health care check-up. In the upstream-dominant lesion at mid-LAD, the upstream APS was higher than the stress in the downstream segment. Approximately 1 year later the

patient developed acute myocardial infarction, and the plaque ruptured at the same location of highest APS in the upstream segment.

Assessment of Lesion Asymmetry with RG

We compared two methods of computing RG in patients' coronary artery lesions in order to determine the practical utility of this metric. Both RGs showed the same trend in both upstream- and downstream-dominant lesions (Table 2). In addition, the relationship of APS with both RGs showed an excellent correlation ($r=-0.956$, $p<0.001$ for RG, $r=-0.967$, $p<0.001$ for analytic RG) (Figure 9A and 9B). The Pearson's correlation coefficient between RG and analytic RG was 0.99 ($p<0.001$) with the average absolute difference of 0.0036 ± 0.0115 ($p=0.677$), and interclass correlation was 0.993 ($p<0.001$) (Figure 9C).

Validation of Patient-Specific Model data with Idealized Stenosis Model

Total 264 stenosis models were constructed, and geometric and physiologic parameters of all stenosis models were presented in Table 5. The mean reference diameter was 3.25 ± 0.56 mm, and mean minimum lumen diameter (MLD) was 1.46 ± 0.62 mm. The percent diameter stenosis and area stenosis were 55.0 ± 17.2 % and 76.8 ± 15.6%, respectively. The total lesion length was 18.55 ± 7.23mm. The idealized stenosis model showed delta pressure of 22.68 ± 21.01 mmHg and mean FFR_{CT} values was 0.71 ± 0.25. The delta FFR_{CT} (ΔFFR_{CT}) was the difference

of FFR_{CT} values across the stenosis lesions, and mean value of ΔFFR_{CT} was 0.27 ± 0.25 (Table 5).

Among the total of 264 idealized models, 120 models (45.5%) were upstream-dominant lesions with higher upstream RG (0.178 ± 0.090 in upstream, 0.082 ± 0.052 in downstream, $p<0.001$) and 120 lesions (45.5%) were downstream-dominant lesions with higher downstream RG (0.082 ± 0.052 versus 0.178 ± 0.090, $p<0.001$) (Table 6). In upstream-dominant lesions, the upstream APS was significantly higher than downstream APS (17380.43 ± 8093.02 vs. 5835.71 ± 3758.82, $p<0.001$), while the converse was also true in downstream dominant lesions (8143.16 ± 4973.74 vs. 11991.89 ± 6255.90 dyne/cm^2, $p<0.001$) (Table 6).

FFR_{CT} decreased progressively as the stenosis severity increased, regardless of the lesion shape (0.94 ± 0.04, 0.90 ± 0.06, 0.85 ± 0.08, 0.74 ± 0.12, 0.55 ± 0.14, 0.30 ± 0.11 for 30% to 80% diameter stenosis, respectively, $p<0.001$). However, APS was largely dependent upon the shape of lesions assessed by RG. For example, 50% diameter stenosis lesions showed different APS patterns according to RG despite similar FFR values (14928.58 ± 4201.79 in upstream vs. 6873.67 ± 2718.63 dyne/cm^2 in downstream, $p<0.001$ for upstream-dominant lesions, 10927.39 ± 3853.68 in upstream vs. 15369.20 ± 6701.80 dyne/cm^2 in downstream, $p=0.002$ for downstream-dominant lesions) (Figure 10).

In upstream segments, the APS linearly increased as the lesion severity increased. However, downstream APS decreased as stenosis severity exceeded a

certain degree (Figure 11A). With regard to the influence of segmental length, the APS increased as the segmental lesion length was shortened, regardless of the stenosis severity (Figure 11B). To summarize, the results of idealized model showed similar results with those of patients-specific lesions.

Discussion

The assessment of risk for ACS has been one of the most important topics in cardiology for decades (2). However, even among plaques with the same vulnerable features, the hemodynamic forces acting on the plaque can vary and affect the risk of rupture. In an optical coherence tomography study, the thickness of ruptured fibrous cap was thicker in patients with exertion-triggered ACS than those with rest-onset ACS (11). This clinical observation demonstrated the potential role of hemodynamic conditions in the stability of plaques. The present study characterizes the hemodynamic forces acting on plaque and its relationship with the geometry of stenotic lesions in both patients and idealized models. The similar characteristics of hemodynamic force in relation to lesion geometry observed in idealized stenosis models provided an intuitive and simplified explanation for the results obtained from patient lesions (Figure 10 and 11).

Role of Hemodynamic Forces in Plaque Rupture

Previous studies have provided many theoretical and experimental foundations for the mechanisms of plaque progression, transformation, and rupture (1,12,13). Imaging studies have presented several vulnerable plaque features such as thin fibrous cap, microcalcification, large lipid core, active inflammation with macrophage infiltration into the plaque, or well-developed vasa-vasorum (2,14). However, those data are related to the composition and organization of the plaque,

not mechanical forces. Therefore, adding information on the hemodynamic forces acting on those plaques may provide better risk stratification and treatment strategy.

Among the external hemodynamic forces, WSS has, to date, provided important clues for understanding the mechanisms of the initiation and eventual rupture of atherosclerotic plaque (12). WSS is hypothesized to recruit inflammatory cells, and cause vasoconstriction and change in endothelial cell morphology. In this respect, WSS has a particular role in representing the substrate that may contribute to plaque rupture or erosion.

Our study focused on the potential role of APS in plaque rupture and its relationship with lesion geometry. APS could uniquely characterize the stenotic segment and differentiate forces acting on upstream and downstream segments of a plaque. Tanaka, et al. reported that the incidence of downstream plaque rupture was up to 36.1% among all rupture cases (7). Our study found that APS could be higher at the downstream than upstream segment in some lesions. In contrast, WSS and the changes in pressure and FFR were consistently higher in upstream than in downstream segment.

Relationship of APS with Lesion Characteristics

The relationship of APS with lesion severity showed different characteristics depending upon the sub-locations – upstream and downstream segments. Upstream APS linearly increased as lesion severity increased, whereas

downstream APS exhibited a concave shape. This result suggests that the risk of downstream rupture can be lower in severe stenosis (> 60-70% diameter stenosis in our study) as a result of decreased downstream pressure. This phenomenon may explain the reason why TIMI 0 flow was less frequently observed in the downstream rupture cases (7). The significant negative correlation between APS and lesion length in our study provides the explanation for higher incidence of plaque rupture in short and focal lesions than in diffuse ones. When the lesions were divided into upstream-dominant and downstream-dominant lesions, the distribution of APS was significantly different between the two groups despite no significant differences in FFR, % diameter stenosis, and WSS pattern in both groups. Therefore, consideration of APS in addition to current plaque evaluation can provide more comprehensive mechanistic explanations for the plaque rupture including the counterintuitive phenomenon of downstream rupture.

Quantitative Geometric Index: RG and analytic RG

We proposed two methods for measuring RG: The first method, denoted as 'RG', is a simplified definition based on the radius measurements of two discrete locations (starting or ending point, and MLA); the second method, denoted as 'analytic RG', is based on the average of radius change over infinitesimal intervals. The two definitions of RG showed an excellent correlation with each other and also showed excellent correlations with APS in both idealized and patient-specific model.

The two methods may be selectively applied according to the complexity of the plaque morphology. If the radius change varies significantly along the length, analytic RG would be more suitable to reflect plaque asymmetry.

Potential Implications of APS in Clinical Practice

It is well-known that a discrepancy exists between anatomic severity and rupture risk of a plaque (2,15). This discrepancy has provided the impetus for many studies to find high risk features for plaque rupture in patients with coronary artery disease, with emphases on plaque morphology and coronary hemodynamics.

In this study, we explored the potential role of APS in plaque rupture. Our study provided three major perspectives distinct from previous studies. First, APS uniquely characterized the differences in stress acting on upstream and downstream segments of a plaque in contrast with the WSS and pressure changes which were consistently higher in the upstream segments. Further, APS revealed the different pattern of force distribution on the upstream and downstream segments according to the severity of stenosis. Second, the dominance of APS varied according to lesion geometry and this finding can potentially provide an explanation for how plaques can rupture at the downstream segment and why rupture is more frequent in focal lesions than in diffuse ones. Third, APS was different even among the plaques with the same degree of stenosis and same degree of pressure drop, based on the RG.

Although the current study has focused on characterizing the external

hemodynamic forces acting on plaques, it should be remembered that coronary plaque rupture is a complex process that is influenced by diverse factors including cardiac contractility, aortic blood pressure, pulse pressure, coronary spasm and endothelial dysfunction. In addition, inter-patient variations of microcirculatory resistance originated from structural changes of the myocardium or primary microvascular dysfunction might influence the prediction of the total hemodynamic forces acting on plaque. The role of these diverse potential factors still warrant further investigations in addition to the analysis of hemodynamic forces presented herein.

Considering the complex nature of plaque rupture, the following three essential elements should be integrated in order to understand the fundamental mechanism of rupture: composition and organization of plaques including plaque vulnerability; lesion geometry including stenosis severity, segmental lesion length, and RG; and external hemodynamic forces including APS. As noted, plaques can rupture when the stress within the plaque exceeds the strength of the plaque. Although we focused on characterizing the external force acting on the plaque, represented by APS, the external hemodynamic force and lesion geometry would influence the stress within the plaque since the external force and the stress within the plaque should be balanced. Moreover, the lesion geometry as well as composition and organization of plaques would determine the strength of plaques. Therefore, patient-specific evaluation of APS and RG will provide additive information in detecting high-risk plaques, and predicting the potential rupture

location and subsequent clinical significance of the rupture event for specific plaques.

Limitations

Some limitations of this study should be noted. First, although we suggested that APS could provide more reasonable explanations for plaque rupture than other parameters previously reported, we did not present a direct longitudinal causal relationship between the APS and subsequent plaque rupture at the location of high APS. A multicenter clinical study is on-going to investigate the causal relationship. Second, we focused on the hemodynamic and geometric parameters potentially related to plaque rupture, but did not investigate the material properties of plaques (i.e. plaque vulnerability). Third, the present study did not consider the abrupt change in physiologic condition and the impact of mechanical stresses caused by cardiac contraction and relaxation. Further studies using fluid-structure interaction simulation methods incorporating plaque properties and cardiac motion with dynamic changes in heart rate will provide more comprehensive information on the risk of plaque rupture. Lastly, the CFD analysis was based on hyperemic static simulation under assumption of laminar flow and without consideration of pulsatile nature of coronary flow. Therefore, further investigation using pulsatile simulation is warranted.

Conclusion

APS uniquely characterizes the stenotic segment and has a strong correlation with lesion geometry. Clinical application of these hemodynamic and geometric indices may be helpful to assess the future risk of plaque rupture and to determine the treatment strategy for patients with coronary artery disease.

요약 (국문초록)

관상동맥 경화반에 작용하는 혈역학적 외력과 병변의 형태적 특징에 따른 혈역학적 외력의 분포에 대한 분석

이주명

의학과 내과학 전공

서울대학교 의학대학원

연구 배경

관상동맥 동맥경화반의 파열은 급성 관상동맥 증후군의 주된 원인이며, 동맥경화반의 파열은 동맥경화반의 내적 강도보다 동맥경화반에 가해지는 혈역학적 힘이 커질 때 발생한다고 생각된다. 그러나, 대부분의 선행

연구는 동맥경화반 내부의 취약성에 대한 연구가 이루어져 왔고, 동맥경화반에 가해지는 혈역학적 힘에 대한 연구는 이루어지지 않았다.

연구 목적

본 연구는 동맥경화반에 가해지는 혈역학적 힘을 분석하고, 동맥경화반의 형태학적 특징에 따른 혈역학적 힘의 분포와 관계를 살펴봄으로써 동맥경화반 파열 메커니즘을 설명하고자 함이다.

연구 방법

안정형 협심증으로 내원하여 관상동맥 CT와 혈관 조영술, 분획혈류 예비력의 평가를 시행 받은 81명 (114 병변)을 대상 환자 군으로 설정하였다. 이 114 병변에 대해 관상동맥 CT에서 추출한 관상동맥의 3D-모델에 전산유체역학 (computational fluid dynamics) 모델을 적용하여 동맥경화반

에 작용하는 혈역학적 힘을 분석하였고, 이러한 힘의 벡터 중, 종축방향으로 작용하는 힘을 종축 전단력 (axial plaque stress, APS)로 명명 후 minimum lumen area (MLA) 지점을 기준으로 근위부에서 원위부로 작용하는 종축전단력을 upstream APS, 원위부에서 근위부 방향으로 작용하는 힘을 downstream APS로 구분 후 분석하였다. 동맥경화반의 형태학적 특징은 종축방향 비대칭성을 평가하였으며, MLA 지점을 기준으로 근위부 및 원위부의 segmental length에 대한 radius의 변화량을 각각 upstream and downstream radius gradient (RG)로 명명하였다. 모든 협착 병변을 근위부와 원위부의 RG에 따라 upstream-dominant (upstream RG > downstream RG) 와 downstream-dominant (upstream RG < downstream RG) 협착 병변으로 분류하였다.

결과

전체 114 협착 병변에서 33 병변 (28.9%)는 downstream APS가

upstream APS보다절대값이 큰 병변이었고, 이들 협착에서 전체 힘의 밸런스는 원위부에서 근위부로 작용하는 방향이었다. 협착 병변의 위중도에 따른 APS의 분포는 upstream 과 downstream APS에서 각각 가른 패턴으로 확인 되었는데, upstream APS의 경우 협착 정도가 심해질수록 선형으로 증가되는 양상이었고, downstream APS의 경우는 협착이 60-70%보다 심해지면 오히려 감소되는 경향을 보였다. 또한 APS는 병변의 길이가 길어질수록 음의 상관관계를 보였다 ($r=-0.274$, $p=0.003$). 협착 병변의 종축 비대칭성과 관계없이 CT로 측정한 분획혈류예비력 (CT-derived fractional flow reserve, FFR_{CT}), 전단력 (wall shear stress, WSS), 압력 차 (pressure gradient)는 모두 upstream segment에서 유의하게 높았다. 그러나 종축전단력의 분포는 협착병변의 종축 비대칭성에 따라 분포에 유의한 차이를 보였는데, upstream-dominant lesion의 경우 upstream APS가 downstream APS에 비해 유의하게 높았고 (11371.96 ± 5575.14 vs. 6878.14 ± 4319.51 dyne/cm^2, $p<0.001$), downstream-dominant lesion의 경우 downstream APS가 upstream APS에 비해 유의하게 높았다

(7681.12 ± 4556.99 vs. 11990.55 ± 5556.64 dyne/cm^2, p<0.001). Upstream-dominant lesion과 downstream-dominant lesion은 FFR_{CT}, % diameter stenosis, 전단력의 분포 (WSS distribution)에서 유의한 차이가 없었지만, 종축 전단력의 분포는 협착 병변의 종축 비대칭성에 따라 유의한 차이를 보였다.

결론

본 연구에서 제시된 종축 전단력은 협착 병변의 형태학적 특징 (종축 비대칭성, 협착의 정도, 병변의 길이)과 유의한 상관관계를 보였고, 기존의 FFR_{CT}, % diameter stenosis, 압력 차, 전단력 등의 개념으로는 구분할 수 없었던 종축 비대칭성을 지닌 협착을 효과적으로 분류할 수 있었다. 협착 병변의 종축 비대칭성에 따른 종축 전단력의 상대적 분포는 동맥경화반 파열이 보다 잘 일어날 수 있는 위치를 시사하며 이런 새로운 개념을 기존의 파열메커니즘의 통념에 적용 시 보다 설명력이 높은 메커니즘을 제

시 할 수 있음을 시사한다.

주요어

관상동맥질환 (coronary artery disease); 종축 전단력 (axial plaque stress); 전단력 (wall shear stress); 압력 (pressure); 동맥경화반 (coronary plaque); 전산유체역학 (computational fluid dynamics); 관상동맥 조영 CT (coronary computed tomography angiography).

학번: 2014-30606

References

1. Fukumoto Y, Hiro T, Fujii T et al. Localized elevation of shear stress is related to coronary plaque rupture: a 3-dimensional intravascular ultrasound study with in-vivo color mapping of shear stress distribution. J Am Coll Cardiol 2008;51:645-50.
2. Stone GW, Maehara A, Lansky AJ et al. A prospective natural-history study of coronary atherosclerosis. N Engl J Med 2011;364:226-35.
3. Li ZY, Howarth SP, Tang T, Gillard JH. How critical is fibrous cap thickness to carotid plaque stability? A flow-plaque interaction model. Stroke 2006;37:1195-9.
4. Li ZY, Gillard JH. Plaque rupture: plaque stress, shear stress, and pressure drop. J Am Coll Cardiol 2008;52:1106-7; author reply 1107.
5. Dolan JM, Kolega J, Meng H. High wall shear stress and spatial gradients in vascular pathology: a review. Ann Biomed Eng 2013;41:1411-27.
6. Samady H, Eshtehardi P, McDaniel MC et al. Coronary artery wall shear stress is associated with progression and transformation of atherosclerotic plaque and arterial remodeling in patients with coronary artery disease. Circulation 2011;124:779-88.
7. Tanaka A, Shimada K, Namba M et al. Relationship between longitudinal morphology of ruptured plaques and TIMI flow grade in acute coronary syndrome: a three-dimensional intravascular ultrasound imaging study. Eur Heart J 2008;29:38-44.

8. Doriot PA. Estimation of the supplementary axial wall stress generated at peak flow by an arterial stenosis. Phys Med Biol 2003;48:127-38.

9. Taylor CA, Fonte TA, Min JK. Computational fluid dynamics applied to cardiac computed tomography for noninvasive quantification of fractional flow reserve: scientific basis. J Am Coll Cardiol 2013;61:2233-41.

10. Taylor AJ, Cerqueira M, Hodgson JM et al. ACCF/SCCT/ACR/AHA/ASE/ASNC/NASCI/SCAI/SCMR 2010 Appropriate Use Criteria for Cardiac Computed Tomography. A Report of the American College of Cardiology Foundation Appropriate Use Criteria Task Force, the Society of Cardiovascular Computed Tomography, the American College of Radiology, the American Heart Association, the American Society of Echocardiography, the American Society of Nuclear Cardiology, the North American Society for Cardiovascular Imaging, the Society for Cardiovascular Angiography and Interventions, and the Society for Cardiovascular Magnetic Resonance. J Cardiovasc Comput Tomogr 2010;4:407 e1-33.

11. Tanaka A, Imanishi T, Kitabata H et al. Morphology of exertion-triggered plaque rupture in patients with acute coronary syndrome: an optical coherence tomography study. Circulation 2008;118:2368-73.

12. Kwak BR, Back M, Bochaton-Piallat ML et al. Biomechanical factors in atherosclerosis: mechanisms and clinical implicationsdagger. Eur Heart J 2014;35:3013-3020.

13. Li ZY, Gillard JH. Plaque rupture: plaque stress, shear stress, and pressure

drop. J Am Coll Cardiol 2008;52:499-500; author reply 500.

14. Otsuka F, Joner M, Prati F, Virmani R, Narula J. Clinical classification of plaque morphology in coronary disease. Nat Rev Cardiol 2014;11:379-89.

15. De Bruyne B, Fearon WF, Pijls NH et al. Fractional Flow Reserve-Guided PCI for Stable Coronary Artery Disease. N Engl J Med 2014.

Figure Legends

Figure 1. Axial Plaque Stress and Other Hemodynamic Parameters

The axial plaque stress (APS) was computed by extracting the axial component of traction acting on the lumen or plaque. Although the magnitudes of traction and FFR decreased along the vessel length, APS uniquely characterized the elevation of hemodynamic stress at upstream and downstream obstructive segments. Note that the magnitude of APS was significantly greater than that of wall shear stress.

Abbreviations: APS, axial plaque stress; FFR, fractional flow reserve; WSS, wall shear stress

Figure 2. Derivation and Definition of Two Different Metrics of Radius Gradient

(A) Definition of the radius gradient (RG). The RG was defined by the radius change over lesion length, where radius change refers to the difference between lesion starting (or ending) point radius and the radius at the location of minimal lumen area (MLA), and lesion length is defined by the length from the lesion starting (or ending) point to MLA location **(B)** Definition of analytic RG. Since there may be substantial variations in each lesion, RG was also analytically computed – analytic RG – by the average of the radius change over infinitesimal intervals.

Figure 3. Distribution of Axial Plaque Stress in Idealized Stenosis Models and Patients Lesions

The distribution of the axial plaque stress in the idealized stenosis model (A) and the patient's lesions (B) are presented.

Figure 4. Distribution of Wall Shear Stress

The distribution of wall shear stress in patient lesions is presented.

Figure 5. Relationship of Axial Plaque Stress with Pressure Gradient

A linear correlation was observed between axial plaque stress and pressure gradient in upstream segments but not in downstream segments due to minimal pressure drop in downstream.

Figure 6. Influence of Lesion Severity and Lesion Length on Axial Plaque Stress

(A) The changes in APS according to the lesion severity (percent diameter stenosis) were presented in the patient's lesions. The upstream APS increased as the stenosis

severity increased while the downstream APS reached maximum at approximately 60% diameter stenosis and decreased as the lesion severity increased. **(B)** APS increased as the segmental length decreased. In addition, APS was also higher when the stenosis severity increased in any given lesion length.

Abbreviations: APS, axial plaque stress; %DS, percent diameter stenosis.

Figure 7. Influence of Lesion Geometry on Hemodynamic Parameters

When upstream-dominant and down-stream dominant lesions were compared, there were no significant differences in FFR_{CT} and % diameter stenosis. However, APS exhibited significant changes according to the lesion geometry. In upstream segments, APS of upstream-dominant lesions was significantly higher than that of downstream-dominant lesions. In downstream segments, APS of downstream-dominant lesions were significantly higher than that of upstream-dominant lesions.

Abbreviations: APS, axial plaque stress; FFR_{CT}, coronary CT angiography-derived fractional flow reserve; WSS, wall shear stress.

Figure 8. Representative Case of Upstream-dominant Lesion

(A) This patient had undergone coronary CT-angiography as routine health care check-up. At that time the patient did not have any symptoms. **(B)** The coronary CT-

angiography showed upstream-dominant lesion (upstream RG > downstream RG) in mid-LAD, and the upstream APS was significantly higher than downstream APS. **(C)** About 1 year later, he developed acute myocardial infarction, and IVUS showed plaque rupture at the same location of highest APS in upstream segment of the plaque.

Abbreviations: APS, axial plaque stress; WSS, wall shear stress

Figure 9. Correlation of Axial Plaque Stress with Two Different Metrics of Radius Gradient

(A) The correlation between axial plaque stress and radius gradient in the patients lesions. **(B)** The correlation between axial plaque stress and analytic radius gradient in the patients' lesions. There were strong correlations between axial plaque stress and two different radius gradient metrics in patients' lesions. **(C)** The correlation of radius gradient and analytic radius gradient in the patient lesions. The Pearson's correlation coefficient was 0.99 ($p<0.001$) with the average absolute difference of 0.0036 ± 0.0115 ($p=0.677$), and interclass correlation was 0.993 ($p<0.001$).

Abbreviations: RG, radius gradient.

Figure 10. Demonstration of Hemodynamic Parameter Changes According to Lesion Severity and Shape in Idealized Models

(A) Lesion severity influenced the APS as well as the other hemodynamic parameters (FFR and WSS). As the lesion severity increased, the upstream APS proportionally increased while downstream APS decreased from 70% diameter stenosis due to decreased pressure in the downstream segment. The magnitude of APS was significantly greater than that of WSS, regardless of the lesion severity.

(B) Lesion shape influenced the APS despite no significant changes in FFRCT and WSS. Due to the same lesion severity (50% DS), no significant changes were observed in FFRCT and WSS. However, the model with highest upstream RG (left) showed the highest upstream APS while the model with highest downstream RG (right) showed the highest downstream APS. Note that upstream APS of downstream-dominant model (right) was similar to upstream APS of symmetric model (middle) since both segments had the same RG values (i.e., 0.146). Likewise, downstream APS of upstream-dominant model (left) was similar to downstream APS of symmetric model (middle) due to the same RG values (i.e., 0.146)

Abbreviations: APS, axial plaque stress; FFRCT, coronary CT angiography-derived fractional flow reserve; %DS, percent diameter stenosis; WSS, wall shear stress

Figure 11. Influence of Stenosis Severity and Lesion Length on Axial Plaque Stress in Idealized Stenosis Models

(A) Impact of Stenosis Severity on APS. The changes in APS according to the lesion severity (percent diameter stenosis) were presented in the idealized model.

The upstream APS increased as the stenosis severity increased while the downstream APS reached maximum at approximately 60% diameter stenosis and decreased as the lesion severity increased. **(B)** Impact of Lesion Length on APS. APS increased as the segmental length decreased. In addition, APS was also higher when the stenosis severity increased in any given segmental lesion length.

Abbreviations: APS, axial plaque stress; %DS, percent diameter stenosis.

Tables

Table 1. Baseline characteristics of the patients

Patients (n = 81)	
Age, years	63.76 ± 9.02
Female gender	12 (15.0%)
Body mass index, kg/m^2	24.54 ± 2.07
Median interval between cCTA and ICA, days	29
Lesion characteristics (n = 114)	
Lesion location	
Left main to LAD	72 (64.0%)
LCX	19 (16.7%)
RCA	22 (19.3%)
cCTA	
Minimal lumen area, mm^2	2.04 ± 0.94
% area stenosis	61.98 ± 13.14
Distance from coronary ostium to MLA, mm	40.39 ± 16.77
Lesion length, mm	14.25 ± 5.52
FFR_{CT}	0.78 ± 0.12
Invasive FFR	0.79 ± 0.11

Values given as mean ± standard deviation or number (percentage), unless otherwise indicated.

Abbreviations: cCTA, coronary computed tomography angiography; FFR_{CT}, coronary CT angiography-derived fractional flow reserve; FFR, fractional flow reserve; ICA, invasive coronary angiography; LAD, left anterior descending coronary artery; LCX, left circumflex artery; RCA, right coronary artery.

Table 2. Distribution of hemodynamic parameters according to the net balance of radius gradient of the lesions in patients with coronary artery disease

Patients model (Total N=114)	*Upstream-dominant lesions (N=56, 49.1%)*			*Downstream-dominant lesions (N=58, 50.9%)*		
	Upstream	**Downstream**	***p* value**	**Upstream**	**Downstream**	***p* value**
Radius gradient	0.11 ± 0.05	0.06 ± 0.03	<0.001	0.07 ± 0.03	0.12 ± 0.05	<0.001
Radius gradient, analytic	0.10 ± 0.04	0.06 ± 0.03	<0.001	0.07 ± 0.03	0.12 ± 0.06	<0.001
Δpressure, mmHg	9.75 ± 8.84	0.18 ± 2.25	<0.001	11.51 ± 8.62	0.69 ± 1.15	<0.001
ΔFFR_{CT}	0.10 ± 0.09	0.002 ± 0.02	<0.001	0.12 ± 0.09	0.01 ± 0.01	<0.001
Pressure gradient, $mmHg/cm^2$	14.72 ± 15.48	0.47 ± 1.83	<0.001	11.62 ± 9.26	1.26 ± 2.50	<0.001
WSS, $dyne/cm^2$	273.49 ± 181.38	147.77 ± 91.84	<0.001	270.90 ± 124.21	153.66 ± 104.89	<0.001
APS, $dyne/cm^2$	11371.96 ± 5575.14	6878.14 ± 4319.51	<0.001	7681.12 ± 4556.99	11990.55 ± 5556.64	<0.001

Values given as mean ± standard deviation.

Abbreviations: APS, axial plaque stress; FFR_{CT}, coronary CT angiography-derived fractional flow reserve; WSS, wall shear stress.

Table 3. Lesion shape and hemodynamic parameters according to the net balance of radius gradient in lesions with % diameter stenosis more than 40%

Patients model	***Upstream-dominant stenosis (N=28, 52.8%)***			***Downstream-dominant stenosis (N=25, 47.2%)***		
(Total N=53)	**Upstream**	**Downstream**	***p* value**	**Upstream**	**Downstream**	***p* value**
Radius gradient	0.13 ± 0.05	0.07 ± 0.024	<0.001	0.08 ± 0.04	0.13 ± 0.05	<0.001
Radius gradient, analytic	0.12 ± 0.04	0.07 ± 0.024	<0.001	0.08 ± 0.04	0.13 ± 0.05	<0.001
Δpressure, mmHg	12.85 ± 10.32	0.10 ± 3.01	<0.001	17.46 ± 9.03	1.26 ± 1.32	<0.001
ΔFFR_{CT}	0.13 ± 0.09	0.002 ± 0.030	<0.001	0.18 ± 0.10	0.01 ± 0.01	<0.001
Pressure gradient, mmHg/cm^2	17.79 ± 17.30	0.40 ± 2.168	<0.001	14.97 ± 11.70	2.01 ± 2.59	<0.001
WSS, dyne/cm^2	296.14 ± 183.45	159.03 ± 94.02	<0.001	291.66 ± 136.77	162.24 ± 126.23	<0.001
APS, dyne/cm^2	14157.72 ± 6086.81	7553.40 ± 3063.96	<0.001	8897.97 ± 4256.20	12870.89 ± 5008.30	<0.001

Values given as mean ± standard deviation.

Abbreviations: APS, axial plaque stress; FFR_{CT}, coronary CT angiography-derived fractional flow reserve; WSS, wall shear stress.

Table 4. Distribution of hemodynamic parameters according to the classifications of net balance in radius gradient of the lesions in patients with coronary artery disease

Patients model (Total N=114)	*Upstream-dominant lesions (N=39, 34.2%)*			*Symmetric lesions (N=38, 33.3%)*			*Downstream-dominant lesions (N=37, 32.5%)*		
	Upstream	**Downstream**	***p* value**	**Upstream**	**Downstream**	***p* value**	**Upstream**	**Downstream**	***p* value**
Radius gradient	0.12 ± 0.05	0.05 ± 0.02	<0.001	0.08 ± 0.03	0.08 ± 0.04	0.617	0.06 ± 0.03	0.13 ± 0.06	<0.001
Radius gradient, analytic	0.11 ± 0.04	0.05 ± 0.03	<0.001	0.08 ± 0.03	0.08 ± 0.04	0.141	0.06 ± 0.03	0.13 ± 0.06	<0.001
Δpressure, mmHg	10.74 ± 9.43	0.12 ± 2.61	<0.001	9.30 ± 6.81	0.59 ± 1.07	<0.001	11.93 ± 9.69	0.63 ± 1.23	<0.001
ΔFFR_{CT}	0.11 ± 0.09	0.002 ± 0.03	<0.001	0.10 ± 0.07	0.01 ± 0.01	<0.001	0.12 ± 0.09	0.01 ± 0.01	<0.001
Pressure gradient, $mmHg/cm^2$	17.30 ± 17.61	1.40 ± 1.59	<0.001	10.37 ± 6.37	1.37 ± 0.95	<0.001	11.66 ± 10.48	2.11 ± 2.37	<0.001
WSS, $dyne/cm^2$	299.58 ± 201.10	157.06 ± 99.69	<0.001	247.03 ± 110.52	140.85 ± 83.46	<0.001	269.11 ± 134.01	154.31 ± 111.91	<0.001
APS, $dyne/cm^2$	12532.31 ± 5895.62	6271.49 ± 3731.99	<0.001	8700.48 ± 3820.97	9716.16 ± 5476.64	0.160	7106.92 ± 4788.62	12616.89 ± 5587.94	<0.001

Values given as mean ± standard deviation.

Abbreviations: APS, axial plaque stress; FFR_{CT}, coronary CT angiography-derived fractional flow reserve; WSS, wall shear stress.

Table 5. Baseline lesion characteristics of the idealized model

Total number	264
Geometric parameters	
Reference diameter, mm	3.25 ± 0.56
Minimum lumen diameter, mm	1.46 ± 0.62
Diameter stenosis, %	55.03 ± 17.15
Area stenosis, %	76.84 ± 15.63
Lesion length, mm	18.55 ± 7.23
Hemodynamic parameters	
FFR	0.71 ± 0.25
Δpressure, mmHg	22.68 ± 21.01
Pressure gradient, mmHg/cm^2	7.05 ± 6.09
ΔFFR	0.27 ± 0.25

Abbreviations: FFR_{CT}, coronary CT angiography-derived fractional flow reserve.

Table 6. Lesion geometry and hemodynamic parameters in the idealized model

	Upstream-dominant stenosis (N=120, 45.5%)			*Downstream-dominant stenosis (N=120, 45.5%)*		
	Upstream	**Downstream**	***p* value**	**Upstream**	**Downstream**	***p* value**
Radius gradient	0.18 ± 0.09	0.08 ± 0.05	<0.001	0.08 ± 0.05	0.18 ± 0.09	<0.001
Radius gradient, analytic	0.18 ± 0.09	0.08 ± 0.05	<0.001	0.08 ± 0.05	0.18 ± 0.09	<0.001
Δpressure, mmHg	26.43 ± 25.21	4.82 ± 5.05	<0.001	27.74 ± 25.05	3.84 ± 3.58	<0.001
ΔFFR_{CT}	0.31 ± 0.30	0.06 ± 0.06	<0.001	0.33 ± 0.30	0.05 ± 0.04	<0.001
Pressure gradient, mmHg/cm^2	25.81 ± 21.22	2.91 ± 2.84	<0.001	13.26 ± 11.73	4.13 ± 3.16	<0.001
WSS, dyne/cm^2	274.39 ± 129.44	28.51 ± 21.67	<0.001	196.25 ± 97.70	11.39 ± 11.77	<0.001
APS, dyne/cm^2	17380.43 ± 8093.02	5835.71 ± 3758.82	<0.001	8143.16 ± 4973.74	11991.89 ± 6255.90	<0.001

Values given as mean ± standard deviation.

Abbreviations: APS, axial plaque stress; FFR_{CT}, coronary CT angiography-derived fractional flow reserve; WSS, wall shear stress.

Figure 1. Axial Plaque Stress and Other Hemodynamic Parameters

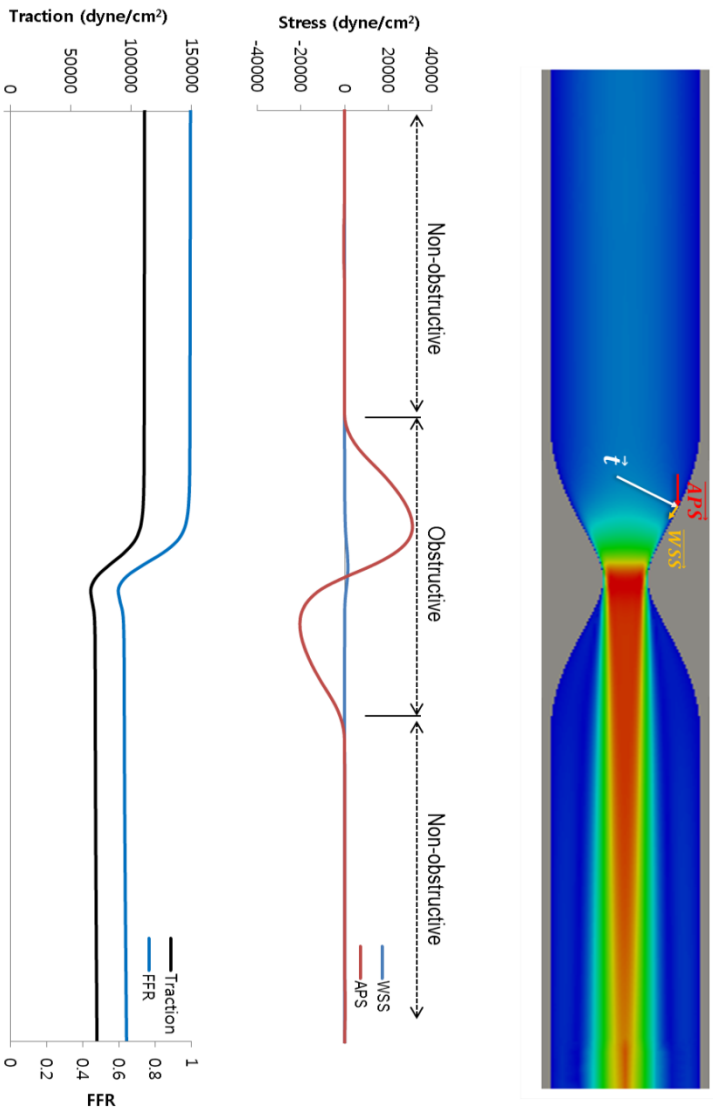

Figure 2. Derivation and Definition of Two Different Metrics of Radius Gradient

A. Definition of Radius Gradient

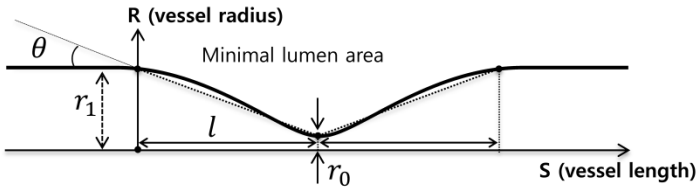

$$RG = \frac{r_1 - r_0}{l}$$

B. Definition of Analytic Radius Gradient

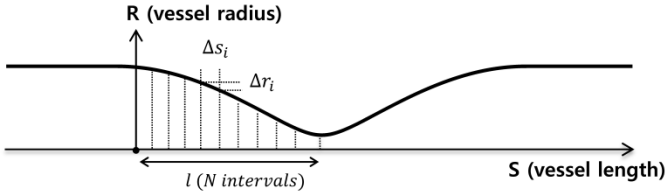

$$analytic\ RG = \frac{1}{N}\sum_{i=1}^{N}\frac{\Delta r_i}{\Delta s_i}$$

Figure 3. Distribution of Axial Plaque Stress in Idealized Stenosis Models and Patient Lesions

A. Idealized Model

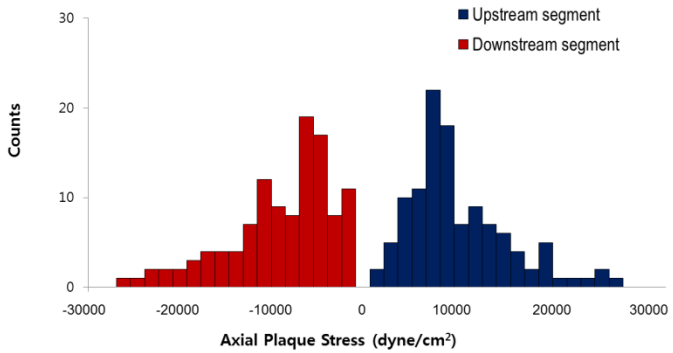

B. Patient Lesions

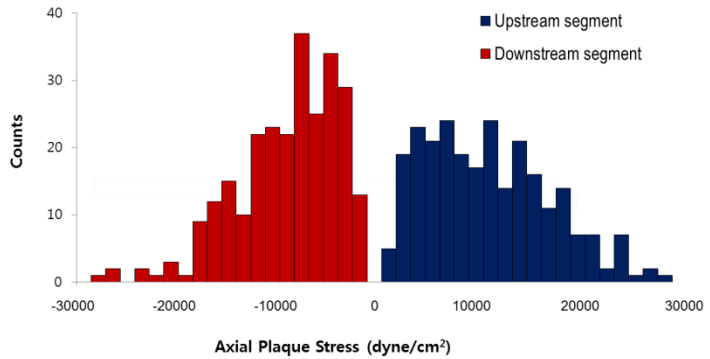

Figure 4. Distribution of Wall shear stress

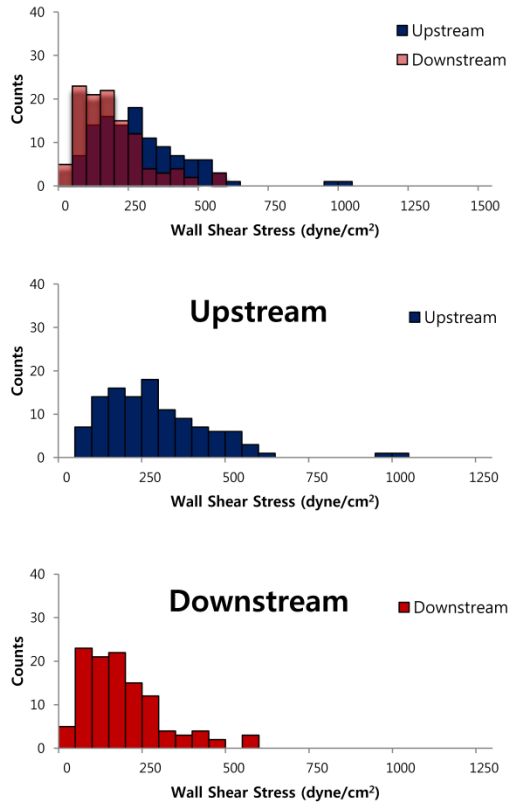

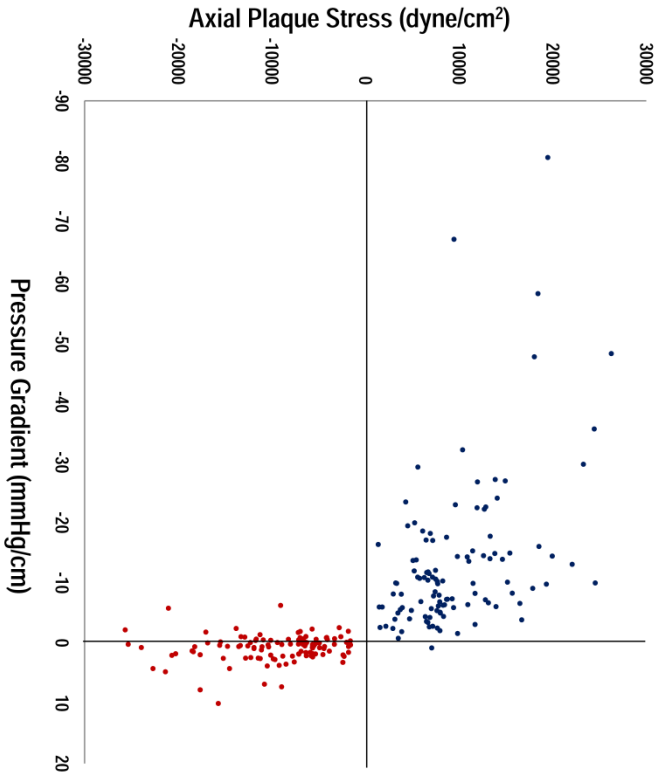

Figure 5. Relationship of Axial Plaque Stress with Pressure Gradient

Figure 6. Influence of Stenosis Severity and Lesion Length on APS

A. Impact of Stenosis Severity on APS

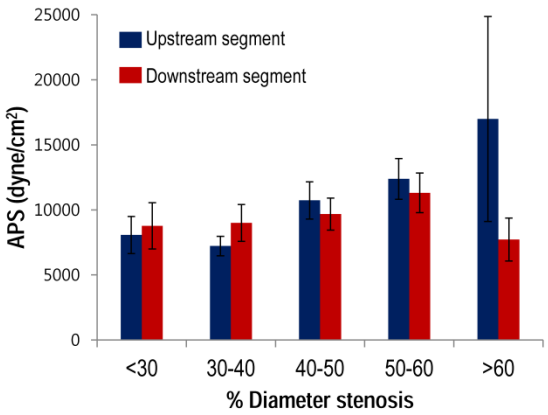

B. Impact of Lesion Length on APS

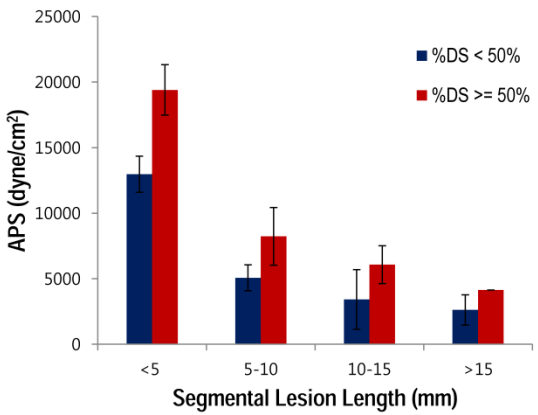

Figure 7. Influence of Lesion Geometry on Hemodynamic Parameters

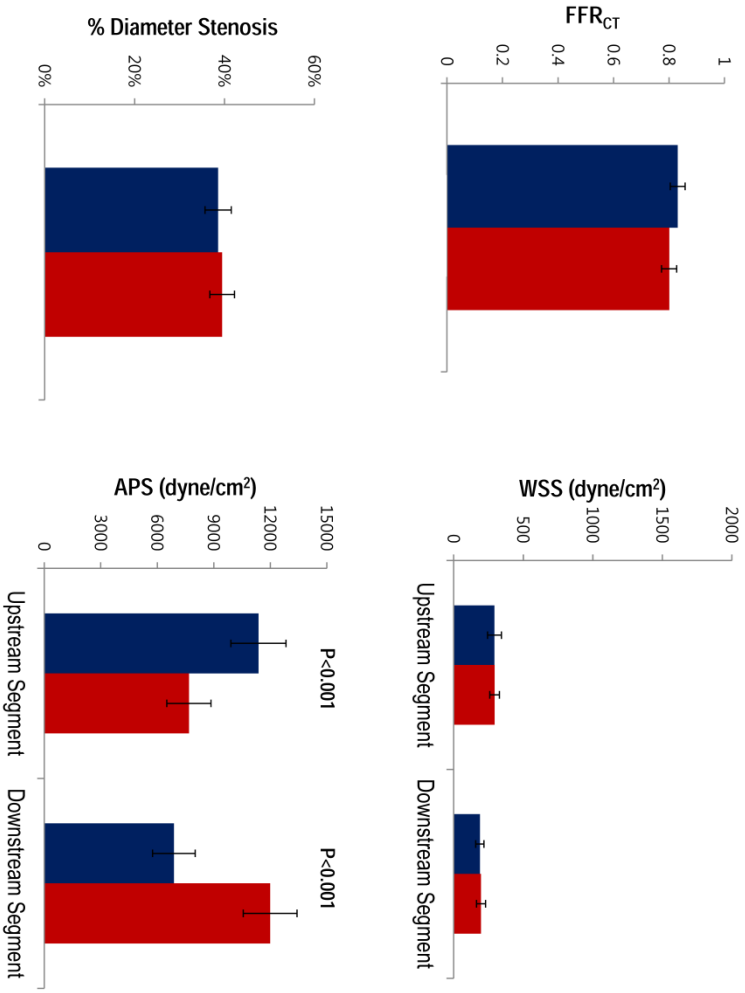

Figure 8. Representative Case of Upstream-dominant Lesion

A

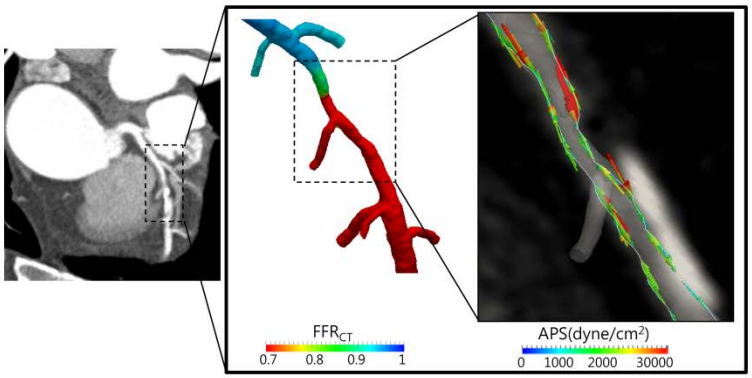

B

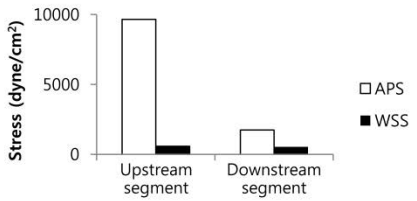

	Upstream segment	Downstream segment
|Radius Gradient|	0.14	0.049
|APS| (dyne/cm^2)	9660	1740
|WSS| (dyne/cm^2)	563	525

C

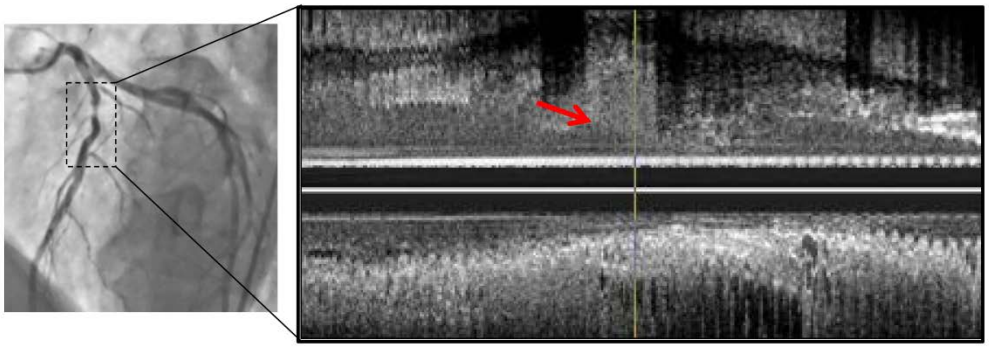

Figure 9. Correlation of Axial Plaque Stress with Two Different Metrics of RG

A. Correlation of APS to RG

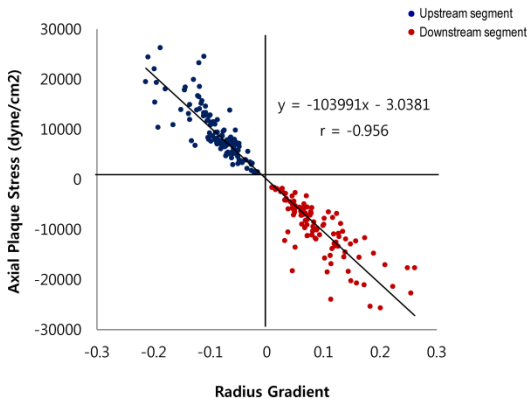

B. Correlation of APS to Analytic RG

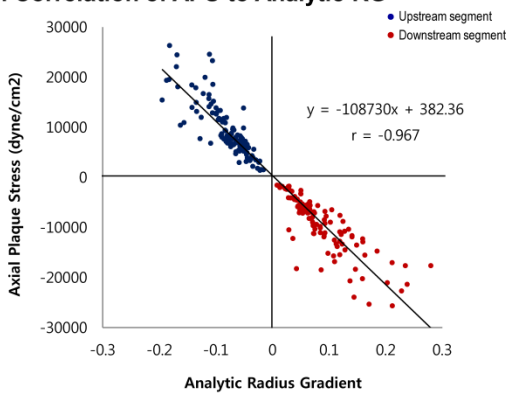

C. Correlation of RG to analytic RG in patients

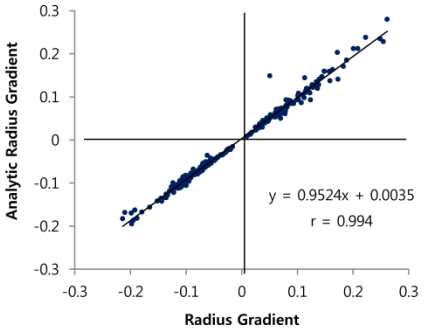

Figure 10. Demonstration of Hemodynamic Parameter Changes According to Lesion Severity and Shape in Idealized Models

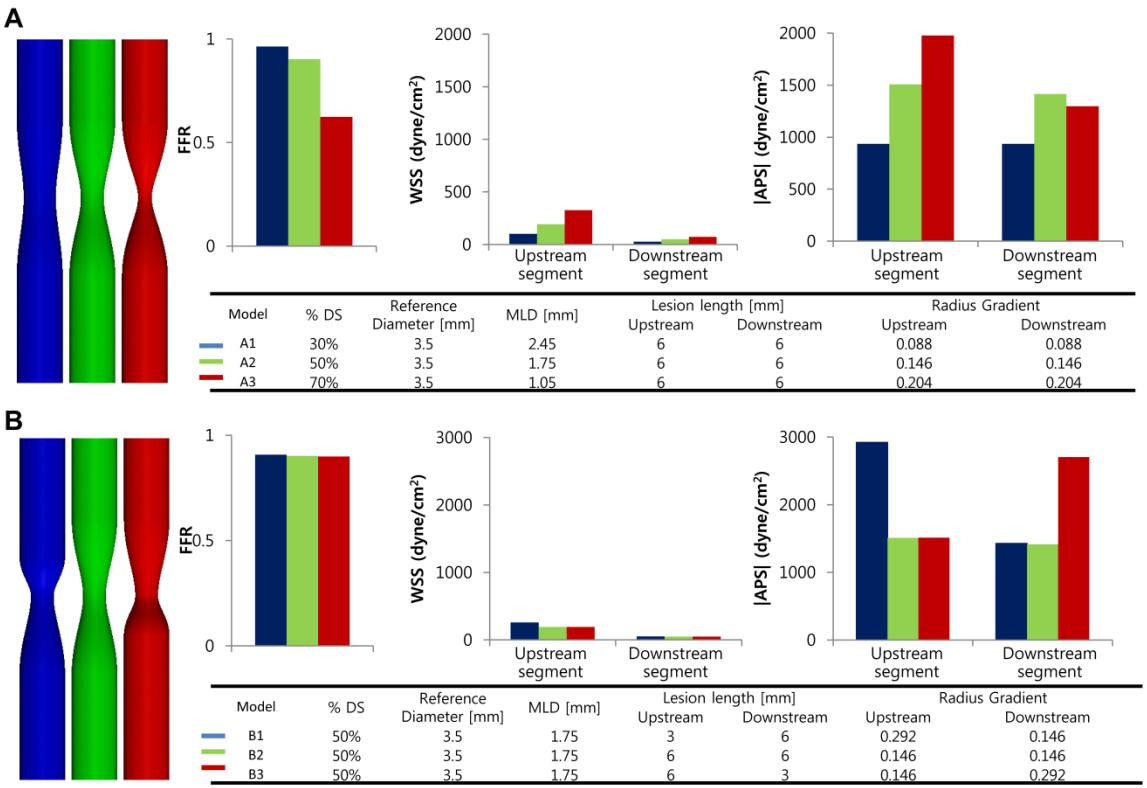

Model	% DS	Reference Diameter [mm]	MLD [mm]	Lesion length [mm] Upstream	Lesion length [mm] Downstream	Radius Gradient Upstream	Radius Gradient Downstream
A1	30%	3.5	2.45	6	6	0.088	0.088
A2	50%	3.5	1.75	6	6	0.146	0.146
A3	70%	3.5	1.05	6	6	0.204	0.204

Model	% DS	Reference Diameter [mm]	MLD [mm]	Lesion length [mm] Upstream	Lesion length [mm] Downstream	Radius Gradient Upstream	Radius Gradient Downstream
B1	50%	3.5	1.75	3	6	0.292	0.146
B2	50%	3.5	1.75	6	6	0.146	0.146
B3	50%	3.5	1.75	6	3	0.146	0.292

Figure 11. Influence of Stenosis Severity and Lesion Length on APS in Idealized Stenosis Models

A. Impact of Stenosis Severity on APS

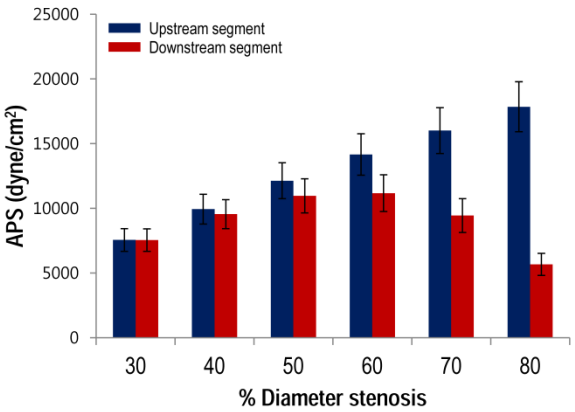

B. Impact of Lesion Length on APS